



The architecture of hydrogen and sulfur σ -hole interactions explain differences in the inhibitory potency of C- β -D-glucopyranosyl thiazoles, imidazoles and an N- β -D glucopyranosyl tetrazole for human liver glycogen phosphorylase and offer new insights to structure-based design

Efthimios Kyriakis^a, Aikaterini G. Karra^a, Olga Papaioannou^a, Theodora Solovou^a, Vassiliki T. Skamnaki^a, Panagiota G.V. Liggri^{b,c}, Spyros E. Zographos^c, Eszter Szennyes^b, Éva Bokor^b, Sándor Kun^b, Anna-Maria G. Psarra^{a,*}, László Somsák^{b,*}, Demetres D. Leonidas^{a,*}

^a Department of Biochemistry and Biotechnology, University of Thessaly, Biopolis, 41500 Larissa, Greece

^b Department of Organic Chemistry, University of Debrecen, H-4002 POB 400 Debrecen, Hungary

^c Institute of Chemical Biology, National Hellenic Research Foundation, 48 Vassileos Constantinou Avenue, 11635 Athens, Greece

ABSTRACT

C-Glucopyranosyl imidazoles, thiazoles, and an N-glucopyranosyl tetrazole were assessed *in vitro* and *ex vivo* for their inhibitory efficiency against isoforms of glycogen phosphorylase (GP; a validated pharmacological target for the development of anti-hyperglycaemic agents). Imidazoles proved to be more potent inhibitors than the corresponding thiazoles or the tetrazole. The most potent derivative has a 2-naphthyl substituent, a K_i value of 3.2 μ M for hepatic glycogen phosphorylase, displaying also 60% inhibition of GP activity in HepG2 cells, compared to control vehicle treated cells, at 100 μ M. X-Ray crystallography studies of the protein – inhibitor complexes revealed the importance of the architecture of inhibitor associated hydrogen bonds or sulfur σ -hole bond interactions to Asn284 OD1, offering new insights to structure-based design efforts. Moreover, while the 2-glucopyranosyl-tetrazole seems to bind differently from the corresponding 1,2,3-triazole compound, the two inhibitors are equipotent.

1. Introduction

Glycogen phosphorylase (GP) is an allosteric enzyme that catalyses the first step of glycogenolysis in brain, liver and muscle to produce glucose-1-phosphate (Glc-1-P), which is then transformed by other enzymes of the glycolytic pathway to glucose¹. The liver enzyme is mainly responsible for maintaining physiological blood glucose levels (normoglycaemia) and any pathological imbalance of glucose homeostasis such as the one that occurs in diabetes involves an uncontrollable activity of GP¹.

Hepatic GP (hGP) is a validated pharmaceutical target for the development of specific inhibitors for the production of novel anti-hyperglycaemic agents^{2–4}. Since glucose is the physiological inhibitor of GP, inhibitor development is mainly based on glucose derivatives⁵. Several studies^{1,6,7} led to the development of potent inhibitors (K_i in the range of nM) from glucopyranose derivatives with substituents at the C1 position since (i) modification of any other atom of the glucopyranose ring led to weaker inhibitors^{1,8–10}, and (ii) the existence of residues inside a hydrophobic cavity (termed β -channel) within the enzyme's active site offers interactions in the direction of the C1 β -

anomeric substituent,^{11,12}. The β -channel extends by the active site and on one side, it is lined with non-polar residues, Phe285 and Phe286¹³ that create a favourable environment for the binding of non-polar groups. On the other side, polar residues Arg339, His341, and Arg292¹³ favour the binding of polar groups. Binding to the β -channel has also implications for the allosteric transition (T to R state) of GP. This transition lies within a flexible loop (280 s, residues 282–286) whose conformation is controlled by allosteric modulators that bind to GP and stabilize or promote either a “closed” or an “open” conformation of the loop. In the T state (inactive form) the loop adopts the “closed” conformation, that blocks the active site preventing entrance of the substrate. In the R state (active form), the 280 s loop is displaced (“open” conformation) and the catalytic site becomes accessible to the substrate¹. Potent GP inhibitors form an extensive network of polar and non-polar interactions with residues that constitute the β -channel and stabilize the inactive T state conformation of the 280 s loop^{1,5–7}.

Three main groups of potent glucose based inhibitors that also displayed *ex vivo* and *in vivo* efficacy^{3,14–18} have been reported thus far: N- β -D-glucopyranosyl-N'-acyl-ureas⁵, glucopyranosylidene-spiro-heterocycles⁵, and C- β -D-glucopyranosyl heterocycles¹⁹. Among the C-

* Corresponding authors.

E-mail addresses: ampsarra@bio.uth.gr (A.-M.G. Psarra), somsak.laszlo@science.unideb.hu (L. Somsák), ddleonidas@bio.uth.gr (D.D. Leonidas).

<https://doi.org/10.1016/j.bmc.2019.115196>

Received 28 August 2019; Received in revised form 24 October 2019; Accepted 30 October 2019

Available online 14 November 2019

0968-0896/ © 2019 Elsevier Ltd. All rights reserved.

glucopyranosyl heterocycles those with an imidazole or 1,2,4-triazole linker (1–4, Table 2) were significantly successful^{10,20–24} with the most potent 2-naphthyl substituted ones displaying K_i values of 26 (2) and 172 (4) nM for hGp, respectively. Their potencies were attributed to a hydrogen bond interaction of the heterocyclic linker to the main chain carbonyl oxygen of His377 and to van der Waals interactions of the aryl substituent occupying the β -channel^{10,20–23}. These interactions appear to be crucial for potency since more than half of the inhibitors reported thus far, have $K_i > 100 \mu\text{M}$ ^{5,7,25}. A further increase of the number of *N*-atoms in the linker as in *C*-glucopyranosyl tetrazole 5 resulted in an inactive compound²⁶. *N*-Glucopyranosyl azole type compounds were significantly less studied in comparison to their *C*-glucosyl counterparts. While 1- β -D-glucopyranosyl-1,2,3-triazoles e.g. 7^{27,28} proved to be μM inhibitors, 1- β -D-glucopyranosyl-4-phenyl-imidazole 6 was non-inhibitory for rabbit muscle GPb (rmGPb)²⁶. Various substituted 9- β -D-glucopyranosyl purines had K_i -s in the range of 170–2000 μM ²⁹. It is interesting to note that the *C*-glucopyranosyl counterparts of 7 proved inactive when tested with GP²⁶. A most important conclusion of these studies has been that the heterocyclic linkers' constitution¹⁹ and also their type of linkage to the sugar unit (*C*- vs *N*-glycosylic structure) has a decisive influence on the inhibitory activity. Therefore, studying the binding modes of as many heterocyclic conjugates of glucose as possible at high resolution may lead to a deeper understanding of the way of action of such inhibitors.

Herein we focus on *in vitro* kinetic studies with GP enzymes and *ex vivo* investigations in hepatic cells of recently synthesized *C*-glucopyranosyl imidazoles 8, 9¹⁴ and thiazoles 10, 11¹⁴ and 12, 13²⁴ as well as *N*-glucopyranosyl tetrazole 14²⁶. The binding of thiazole compounds 10 and 11 to GP has been recently studied *in silico* and *ex vivo*¹⁴ since the inclusion of sulfur to compounds has been shown to improve cell permeability and sulfur atom is included in a large number of marketed drugs, particularly in the form of heterocycles³⁰. Thus, in our study we included four thiazole analogues to provide further insights to their GP inhibitory potential by kinetics and X-ray crystallography.

Furthermore, an X-ray crystallographic study of the enzyme-inhibitor complexes of the above compounds was carried out to elucidate the differences in the binding strength of isomeric molecules and the alterations observed with analogous structures to further broaden structure-activity relationships of these compound classes.

2. Materials and methods

2.1. Kinetic studies

rmGPb, rmGPa and hGPa were produced and assayed for enzymatic activity as described earlier^{21,31}. Initial velocities were calculated from the pseudo-first order rate constants using the first-order rate equation and inhibition constant (K_i) values were calculated from the plot of $K_{m(\text{app.})}$ vs [inhibitor] using the non-linear regression program GRAFIT³² and an explicit weighting. Inhibitor concentration used were as follows: 5, 10, 20, 25, and 30 μM (8), 1, 2, 3.2, 4 and 5 μM (9), 75, 150, 200, and 300 μM (10), 10, 30, 45, 50 and 60 μM (11), 50, 100, 200, and 250 μM (12), 25, 50, 100, 150, and 200 μM (13), 50, 100, 200, and 300 μM (14).

2.2. Ex vivo studies

Human HepG2 hepatocarcinoma cells were maintained in DMEM, containing 25 mM glucose 10% FBS, 2 mM glutamine, and penicillin/streptomycin. Cells were grown at 37 °C in a humidified atmosphere with 5% CO₂. Treatment and assessment of GP activity were performed as previously described^{33,34}. Briefly, cells were seeded in 60 mm culture dishes at a density of 1.0×10^6 cells per dish. After cell attachment (16–18 h), the medium was replaced by medium containing 10 nM dexamethasone, 25 mM glucose, and 100 nM insulin, and cells were further incubated for 16–18 h to replenish glycogen stores. Then, cells

were incubated for 3 h in the presence or absence of the indicated amounts of the inhibitors 8, 9, and 11 in medium supplemented with 5 mM glucose and 100 nM glucagon to promote glycogenolysis. Subsequently, cells were washed in 150 mM NaCl, 20 mM Tris buffer (pH 7.5), harvested, centrifuged at 700 g for 5 min. Resulting pellets were resuspended in 20 mM Tris (pH 7.5) containing 0.05% Triton, and 1 mM PMSF and subjected to sonication. The lysates were centrifuged in a microcentrifuge at 12,000 g for 30 min. In the supernatants, protein concentration was assessed according to the Bradford method³⁵, and GPb activity, was evaluated as described above. Cytotoxicity of 8, 9 and 11 inhibitors, upon 3 h and 24 h incubation of the cells, was assessed by applying MTT assay, as previously described³⁶. Growth medium and its supplements were purchased from Thermo Fisher Scientific, dexamethasone, glucagon, insulin and MTT was purchased from Sigma-Aldrich.

2.3. X-Ray crystallography

Tetragonal (space group $P4_32_12$) T state rmGPb crystals were grown by the batch method as described previously³¹. X-ray crystallographic binding studies were performed by diffusion of either 8 (10 mM; 18 h), 9 (1 mM; 21 h), 10 (10 mM; 21 h), 11 (10 mM; 21 h), 12 (7.5 mM; 48 h), 13 (1 mM; 24 h), or 14 (10 mM; 21 h) solution in the crystallization media (see above) supplemented with 15% (v/v) DMSO in preformed rmGPb crystals at room temperature prior to data collection. X-Ray diffraction data were collected using a Cu X-ray microfocus source (Oxford Diffraction SuperNova) equipped with a 4 kappa goniometer and the ATLAS CCD (135 mm) detector at room temperature. Crystal orientation, integration of reflections, inter-frame scaling, partial reflection summation, and data reduction was performed by the program CrysAlisPro.³⁷ Scaling and merging of intensities were performed by Aimless³⁸ and the optimum resolution was selected based on the $CC^{1/2}$ criterion.³⁹ Crystallographic refinement of the complexes was performed by maximum-likelihood methods using REFMAC.³⁸ The starting model employed for the refinement of the complexes was the structure of the native T state rmGPb complex determined at 1.9 Å resolution (PDB entry 3L79). Ligand molecule coordinates and topologies were constructed using Coot⁴⁰ and PRODRG⁴¹ and they were fitted to the electron density maps after adjustment of their torsion angles. A summary of the data processing and refinement statistics for the inhibitor complex structures is given in Table 1. The validity of the refinement procedure was checked using the PDB_REDO server⁴². As there were more than five reflections per atom available, both an isotropic and an anisotropic B-factor model were considered, and the isotropic B-factor model was selected based on the Hamilton R ratio test. A TLS model for grouped atom movement with one TLS group was used. The stereochemistry of the protein residues was validated by MolProbity⁴³. Hydrogen bonds and van der Waals interactions were calculated with the program CONTACT as implemented in CCP4³⁸ applying a distance cut off 3.3 Å and 4.0 Å, respectively. Figures were prepared with CCP4 Molecular Graphics⁴⁴. The coordinates of the new structures have been deposited with the RCSB Protein Data Bank (<http://www.rcsb.org/pdb>) with codes presented in Table 1.

3. Results and discussion

3.1. Enzyme kinetic studies

The inhibitory potency of compounds 8–14 was examined against human liver glycogen phosphorylase a (hGPa), and rabbit muscle glycogen phosphorylase a (rmGPa) and b (rmGPb) for comparison to previous studies and to the structural analysis (*vide infra*). The inhibition constant (K_i) values are presented in Table 2. All compounds displayed competitive inhibition with respect to the substrate Glc-1-P as revealed by the Lineweaver-Burk plots that intersect at the same point on the y-axis.

Table 1

Summary of the diffraction data processing and refinement statistics for the rmGPb complexes. Values in parentheses are for the outermost shell.

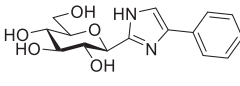
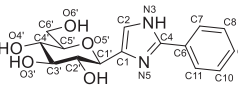
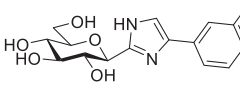
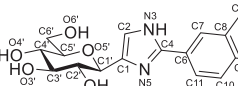
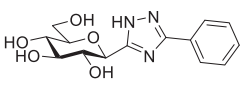
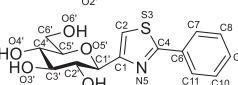
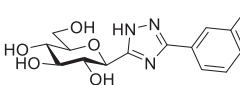
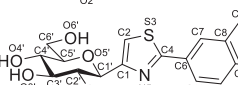
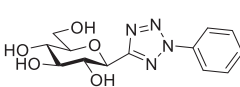
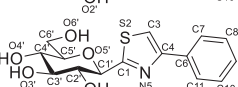
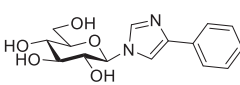
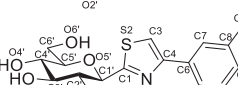
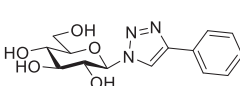
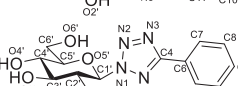
rmGPb complex	8	9	10	11	12	13	14
Resolution (Å)	13.44–2.45	13.70–2.35	13.74–2.37	13.76–2.30	13.52–2.43	13.88–2.37	13.75–2.37
Data collection and processing statistics							
Outermost shell (Å)	2.55–2.45	2.44–2.35	2.46–2.37	2.38–2.30	2.53–2.43	2.46–2.37	2.46–2.37
Reflections measured	195,605 (12,606)	201,013 (12,532)	174,479 (11,177)	211,649 (10,137)	193,893 (13,407)	178,537 (11,494)	184,871 (11,780)
Unique reflections	32,001 (3040)	37,798 (3389)	35,501 (3121)	40,023 (3057)	32,703 (3151)	35,139 (3118)	35,891 (3175)
Multiplicity	6.1 (4.1)	5.3 (3.7)	4.9 (3.6)	5.3 (3.3)	5.9 (4.3)	5.1 (3.7)	5.2 (3.7)
R_{sym}	0.069 (0.344)	0.078 (0.456)	0.077 (0.501)	0.083 (0.597)	0.076 (0.419)	0.085 (0.567)	0.080 (0.567)
Completeness (%)	90.2 (77.9)	93.2 (80.9)	90.5 (77.2)	92.5 (73.8)	90.0 (78.6)	90.0 (77.2)	91.1 (78.1)
$\langle 1/\sigma \rangle$	18.4 (3.6)	13.7 (2.4)	13.9 (2.3)	14.3 (2.0)	16.5 (3.1)	12.6 (2.1)	13.3 (2.0)
$CC^{1/2}$	0.997 (0.929)	0.994 (0.907)	0.996 (0.883)	0.994 (0.802)	0.997 (0.901)	0.996 (0.855)	0.995 (0.826)
Refinement statistics							
R_{cryst}	0.136 (0.187)	0.153 (0.236)	0.153 (0.241)	0.150 (0.233)	0.152 (0.221)	0.154 (0.255)	0.146 (0.237)
R_{free}	0.188 (0.215)	0.208 (0.346)	0.205 (0.279)	0.197 (0.258)	0.211 (0.287)	0.213 (0.348)	0.204 (0.286)
Number of solvent molecules	225	244	171	260	225	229	235
r.m.s. deviation from ideality in							
bonds (Å)	0.007	0.008	0.008	0.008	0.009	0.009	0.012
angles (°)	1.4	1.5	1.5	1.4	1.5	1.5	1.7
Average B factor (Å²)							
Protein atoms	30.2	28.9	30.8	28.8	29.4	31.8	28.9
Solvent molecules	26.2	26.5	24.7	27.9	27.8	28.7	25.5
Inhibitor atoms	16.2	14.8	16.6	33.1	20.7	49.3	15.7
PDB entry	6S4H	6S4O	6S5I	6S4R	6S4K	6S4P	6S5Z

The most potent inhibitor, with K_i values of 3.2 μM and 1.6 μM for hGPa and rmGPa, respectively, is **9**, classifying it as one of the ten most potent GPIs⁷ and the third among the glucopyranosyl-imidazole inhibitors for hGPa discovered thus far²⁰. Although all compounds seem to follow the same potency pattern, as indicated by the K_i values, for all three enzymes (i.e. those more potent for hGPa than others are also

more potent for rmGPa and rmGPb), they all are more potent for rmGPa than for hGPa or rmGPb. The difference of the rmGPb and hGPa K_i values is significant for all inhibitors (apart from **12** and **14**), indicating that these inhibitors can differentiate between the two enzymes. Although this could imply that these inhibitors also bind at another binding site of GP (e.g. the AMP or the inhibitor binding site) with

Table 2

Selected inhibitors of glycogen phosphorylases and the compounds studied here. The crystallographic atom numbering is shown in the inhibitors.

Compound	K_i [μM]			Compound	K_i [μM]		
	rmGPb	rmGPa	hGPa		rmGPb	rmGPa	hGPa
1 	0.280 ²⁴	0.226 ²⁰	0.156 ²⁰	8 	68.6 ^{1,4}	17.7 \pm 0.5	25.9 \pm 0.8
2 	0.031 ²⁴	0.065 ²⁰	0.026 ²⁰	9 	4.58 ^{1,4}	1.6 \pm 0.1	3.2 \pm 0.1
3 	7 ⁴⁵	1.74 ²²	1.35 ²²	10 	326 ^{b,1,4}	75.6 \pm 5.2	172.2 \pm 8.8
4 	0.41 ⁴⁵	0.172 ²²	0.172 ²²	11 	26.2 ^{1,4}	28.0 \pm 1.1	43.6 \pm 1.5
5 	N.I. ^{a,26}	–	–	12 	310 ²⁴	156.9 \pm 13.6	179.9 \pm 5.5
6 	N.I. ^{a,26}	–	–	13 	158 ²⁴	69.1 \pm 3.7	78.0 \pm 2.8
7 	162 ²⁸ 151.3 ²⁷	–	–	14 	162.3 \pm 5.9	146.2 \pm 3.0	134.2 \pm 3.3

^a N.I. No inhibition at 625 μM concentration.

^b Calculated from the IC_{50} value by a web-based tool⁴⁶.

different affinity for the three enzymes, no competition with AMP or caffeine has been observed in kinetic experiments. A possible explanation for this preference might be that the R state conformation of the phosphorylated forms of GP (rmGPa and hGPa) is more sensitive than the R state of the AMP activated rmGPb for these inhibitors.

As expected, 2-naphthyl compounds seem to be more potent than the corresponding phenyl ones (Table 2). Among thiazoles, the most potent is the one with the 2-naphthyl group (11). Isomers 10 and 12, display similar potency for hGPa. However, 2-naphthyl-substituted 11 displays a 1.8 times smaller K_i value than 13. Thiazoles are less potent than their corresponding imidazoles (compare pairs 1–12, 2–13, 8–10, and 9–11) or 1,2,4-triazoles 3 and 4 in Table 2.^{21–23}

Among imidazoles, the 2-naphthyl inhibitor 9 is 8 times more potent than the phenyl 8 (Table 2). However, both are less potent than their isomers 1 and 2, respectively. The *N*-glucopyranosyl tetrazole 14 is the weakest inhibitor in this study. Its inhibitory potency is significantly lower than those of the *C*-glucosyl phenylimidazoles 1 and 8, and 1,2,4-triazole 3. However, comparisons to other *N*-glucopyranosyl azoles show that 14 is more potent than the *N*-glucosyl imidazole 6, and equipotent to the *N*-glucosyl 1,2,3-triazole 7.

Comparing the potencies of the azole inhibitors with a phenyl ring (1, 3, 5, 6, 7, 8, 10, 12, and 14; Table 2) it seems that having a carbon or a nitrogen atom at position 5 (crystallographic numbering; Table 2) does not have a significant impact on potency (7 vs 14) while replacing a carbon by a nitrogen at position 1 or 3 is significantly detrimental to the potency (1 vs 3, 6, 7, and 14). Furthermore, with a single exception (6) increasing the number of nitrogen atoms in the azole linker above two, it seems that decreases the inhibitory potency.

3.2. Ex vivo studies

The inhibitory effect of the three most potent inhibitors 8, 9 and 11 was further evaluated for their efficiency to inhibit GP activity in human hepatocarcinoma HepG2 cells. Pre-treatment of the cells, as described in experimental section, to induce glycogen synthesis, was followed by incubation of the cells with inhibitors 8, 9, and 11, as indicated in Fig. 1, for 3 h, upon glucose deprivation and induction of glycogenolysis. Harvest, lysis of the cells and assessment of GP activity in cell lysate was followed. In accordance with enzyme kinetic studies, inhibitor 9 was the most effective compound in inhibiting GP activity in HepG2 cells, exhibiting approximately 60% inhibition, compared to control vehicle treated cells, at a concentration of 100 μM (Fig. 1). No

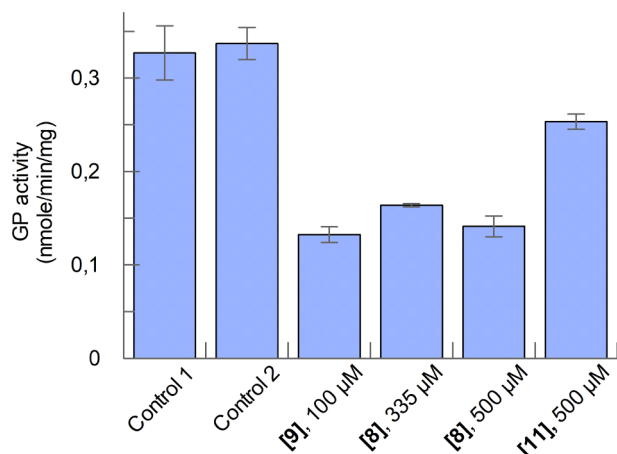


Fig. 1. Evaluation of GP inhibitory activity of 8, 9, and 11 in HepG2 cells. Diagram of GP activity in control reactions (no inhibitor) and in presence of 9 (100 μM), 8 (335 μM , 500 μM) and 11 (500 μM). The activity of GP is expressed as nmol/min/mg of protein. GP activity shown is calculated by linear regression using 5 time points and errors (shown in bars) were obtained by from the error of the fitted slope.

cytotoxicity was observed upon 3 and 24 h incubation of the cells for 100 μM of 9 (Fig. 2).

Approximately 50 and 60% GP inhibition was achieved by 8, at a concentration of 335 and 500 μM , respectively, whereas 11 showed less than 25% inhibition, at the highest concentration of 500 μM . Due to the high cytotoxic effects of 11 (Fig. 2), concentrations higher than 500 μM were not considered. In case of 11, less than 10% decrease in cell viability was observed upon treatment conditions (3 h). Nevertheless, upon 24 h treatment, 8 and 11 exhibited considerable cytotoxicity at concentrations higher than 200 μM (Fig. 2). In conclusion, inhibitor 9 was the most effective in GP inhibition, with no cytotoxic effects.

In a recent publication¹⁴ the effect of compounds 8, 9 and 11 on glucagon-stimulated glycogenolysis in mouse hepatocytes was studied. Inhibitors 9 and 11 caused significant inhibition but with IC_{50} values greater than 100 μM whereas 8 did not produce any significant inhibition at the same concentration. These results agree with our studies with HepG2 cells.

3.3. X-Ray crystallography studies

X-Ray crystallography studies of the rmGPb – inhibitor complexes were performed to analyse the structural basis of their inhibitory potency. The use of rmGPb, was mainly due to the ease in growing suitable crystals for protein-inhibitor complexes. Studies with rmGPb are plausible to hGPa (the pharmaceutical target) as it has been shown in numerous previous studies^{10,20–23,31}, due to the absolute conservation (in terms of sequence of the catalytic site (targeted by these inhibitors) in all mammalian GPs⁴⁷ and in terms of structure between rmGPb and hGPa⁴⁸. The electron density maps (Fig. 3) clearly defined the position of each atom of the seven inhibitors bound at the catalytic site of rmGPb.

Superposition of the complex structures on the structure of free rmGPb over well-defined residues (18–49, 262–312, 326–829) produced r.m.s.d. values of 0.6–0.7 Å for all protein atoms of the inhibitor complexes, indicating that the binding of any of the inhibitors studied, did not trigger any major conformational change on the overall protein structure. However, the binding of 8, 10, and 12, trigger a small but significant perturbation of the 280 s loop (residues 282–289) which is more apparent on Asn284 and Phe285 whose atoms move away on average by 1.0 Å from their position on the native structure. All seven inhibitors bind by anchoring the β -glucopyranose ring at the glucose binding site within the active site similar to previous glucopyranose derivatives^{1,5–7}. By binding there, the hydroxyl groups of the glucopyranose ring engage in a very similar network of hydrogen bond interactions with residues of the active site in all inhibitor complexes (Table 3). The only exception occurs at the 12 complex where O2' is 3.6 Å away from ND2 of Asn284, a rather long distance for a hydrogen bond interaction. This removal appears to be due to a 0.4 Å shift of the Asn284 ND2 atom from the position it occupies in all the six other inhibitor complexes. In all inhibitor complexes three conserved water molecules mediate hydrogen bonds of the glucopyranose hydroxyl groups to Asp283, Asn284, Tyr573, Lys574, Thr671, Ala673, Thr676 and the cofactor PLP (Fig. 4).

In the 8 and the 9 complexes the linker atom N3 (Table 2) is involved in a hydrogen bond interaction with the side chain OD1 of Asn284, while in the 11 and the 13 complexes the other nitrogen (N5) forms a hydrogen bond to the other atom (ND2) of Asn284 (Table 3). In all the other inhibitor complexes the linker atoms are not involved in any hydrogen bond interactions (Fig. 4). However, sulfur, like halogens possesses σ -hole properties which leads to σ -hole bonding similar to halogen bonding⁴⁹. Thus, the heterocyclic sulfur atom of 10 and 11 interacts with Asn284 OD1 while the heterocyclic sulfur atom of 12 and 13 interacts with His377 O and Asn284 OD1 (Table 3). Apart from these interactions the linker atoms of 8, 9, 10, 11, 12, 13, and 14 participate in 11, 17, 15, 19, 17, 15, and 13 van der Waals interactions, respectively, with Leu136, Asn284, His377, and Thr378.

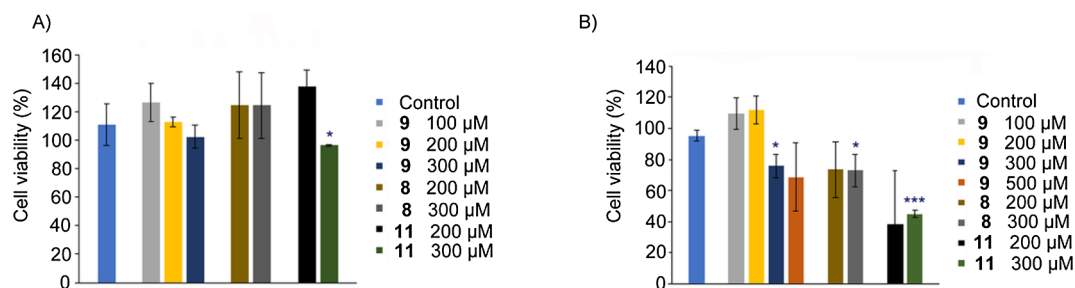


Fig. 2. Percentage inhibition of HepG2 cell viability by **8**, **9** and **11**. Cell viability upon 3 h (A) and 24 h (B) treatment of the cells was measured applying MTT assay and expressed as a percentage of cell viability of control cells, that was set at 100%; Results are expressed as mean \pm SD ($n = 3-5$). Data were analyzed by independent *t*-test. Differences were considered significant at a two tailed P value < 0.05 .

The phenyl rings of **8**, **10**, **12**, and **14** bind very similarly at the active site (Fig. 4) and they engage in 17, 15, 18, and 15 van der Waals interactions, respectively, with protein residues Glu88, Asn282, Asn284, Phe285, and His341. In addition to these interactions the naphthyl rings of **9**, **11**, and **13** form 10, 12, and 14 van der Waals interactions, respectively, with, Glu88, Asn282, Phe285, Arg292, His341, and Ala383. In a recent publication with C- β -D-glucopyranosyl azole type inhibitors of glycogen phosphorylase that reduce glycogenolysis in hepatocytes¹⁴, molecular dynamics have suggested the formation of a salt bridge between the imidazole and the side chain of Asp283 which might contribute to inhibitor binding. In the **8** and **9** complexes the distance of N5 to Asp283 OD1 is 4.5 Å, which is longer by 0.5 Å from the used distance between N–O atom pairs for the definition of salt bridge formation⁵⁰. However, this distance is enough for long range coulombic interactions which have been shown to play an important role in protein-ligand interactions^{51–53} and therefore, the crystal structures of the **8** and **9** complexes are in agreement with the molecular dynamics study¹⁴.

Comparative structural analysis of the binding of thiazoles (**10**, **11**, **12**, and **13**) to rmGPb reveals the structural basis for the significant differences in their inhibitory potency. Thus, **10** forms ten hydrogen bond interactions and one sulfur σ -hole bonding interaction, whereas **12** forms nine hydrogen bond interactions and two sulfur σ -hole bonding interaction (Table 3). Furthermore, they engage in a similar number of van der Waals interactions and are, hence, almost equipotent. Compounds **11** and **13** form one and two additional hydrogen bond and/or sulfur σ -hole bonding interactions (Table 3), respectively, and together with the additional van der Waals contacts formed by the 2-naphthyl ring with respect to those of the phenyl, constitute the structural basis for the significant potency increment with respect to those of **10**, and **12**. The sulfur σ -hole bonding interactions are very similar in length (Table 3) and this reflects the similarity of potency for **10** ($K_i = 172.2 \mu\text{M}$) and **12** ($K_i = 179.9 \mu\text{M}$) or for **11** ($K_i = 43.6 \mu\text{M}$) and **13** ($K_i = 78.0 \mu\text{M}$). The difference in the potency between **11** and **13** might be attributed to the π -stacking interactions between the 2-naphthyl ring and the imidazole ring of His341 (Fig. 5). In the **13**

Table 3

Potential hydrogen bond and sulfur σ -hole bonding interactions of inhibitors with rmGPb residues at the catalytic site in the crystal. Numbers shown are distances in Å.

Inhibitor atoms ^a	Protein atoms	8	9	10	11	12	13	14	
Glucopyranose atoms	O2'	Asn284 (ND2)	3.1	3.0	3.3	3.1	–	3.3	2.7
		Tyr573 (OH)	3.1	3.1	3.1	3.0	3.2	3.0	3.1
		Glu672 (OE1)	3.2	3.2	3.3	3.1	3.3	3.3	3.3
	O3'	Glu672 (OE1)	2.8	2.8	2.8	2.8	2.8	2.8	2.8
		Ala673 (N)	3.3	3.3	3.2	3.2	3.3	3.2	3.2
		Ser674 (N)	3.2	3.1	3.2	3.0	3.2	3.0	3.1
		Gly675 (N)	3.2	3.1	3.2	3.0	3.2	3.1	3.2
	O4'	Gly675 (N)	2.9	2.8	2.9	2.8	2.9	2.8	2.8
	O6'	His377 (ND1)	2.8	2.8	2.8	2.6	2.7	2.6	2.8
		Asn484 (ND2)	2.7	2.6	2.6	2.6	2.7	2.6	2.6
Linker atoms	N3	Asn284 (OD1)	3.3	3.2	–	–	–	–	–
	N5	Asn284 (ND2)	–	–	–	3.2	–	3.3	–
	S2	His377 (O)	–	–	–	–	3.2	3.2	–
		Asn284 (OD1)	–	–	–	–	3.4	3.4	–
	S3	Asn284 (OD1)	–	–	3.3	3.6	–	–	–
Total number of interactions			11	11	11	12	11	13	10

^a For crystallographic atom numbering see Table 2.

complex (Fig. 4), the imidazole ring of His341 forms a single perpendicular π -stacking interaction with the outer ring of the naphthyl substituent (distance between center of charge and aromatic ring center is 3.8 Å), whereas in the **11** complex (Fig. 4) the imidazole of His341 forms two perpendicular π -stacking interactions, one with each of the two aromatic rings of the naphthyl ring, (distances between center of charge and aromatic ring center are 4.0 and 4.4 Å). This π -cation interaction has been observed before with other naphthyl substituted inhibitors to confer to inhibitory potency^{31,54}.

The two imidazole inhibitors, **8** and **9**, are involved in a similar hydrogen bonding and van der Waals interactions network with protein residues (Table 3). The naphthyl ring of **9**, is involved in ten more van der Waals interactions than the phenyl ring of **8** and two instead of one π -perpendicular stacking interactions with the imidazole ring of

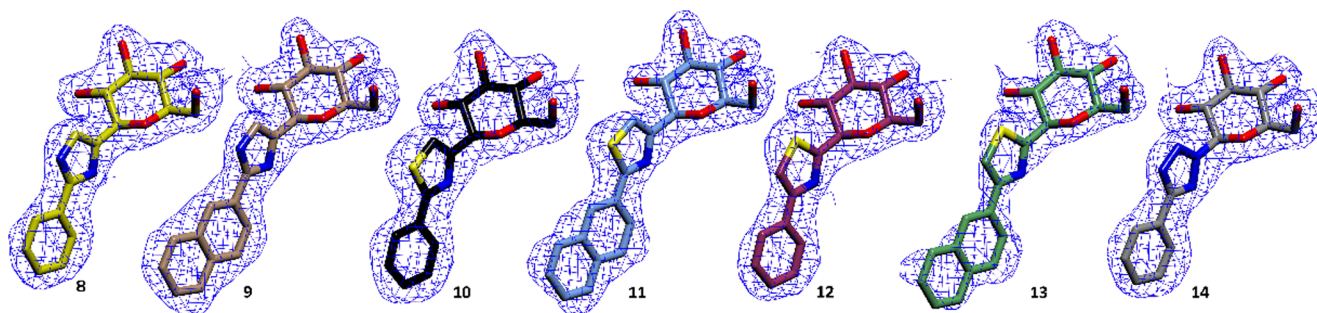


Fig. 3. The REFMAC weighted 2Fo-Fc electron density maps of the bound ligands at the catalytic site (from left to right, **8**, **9**, **10**, **11**, **12**, **13**, and **14**). Maps are contoured at 1.0 σ before the incorporation of the ligand molecules in the refinement process and the final models of the inhibitors are shown.

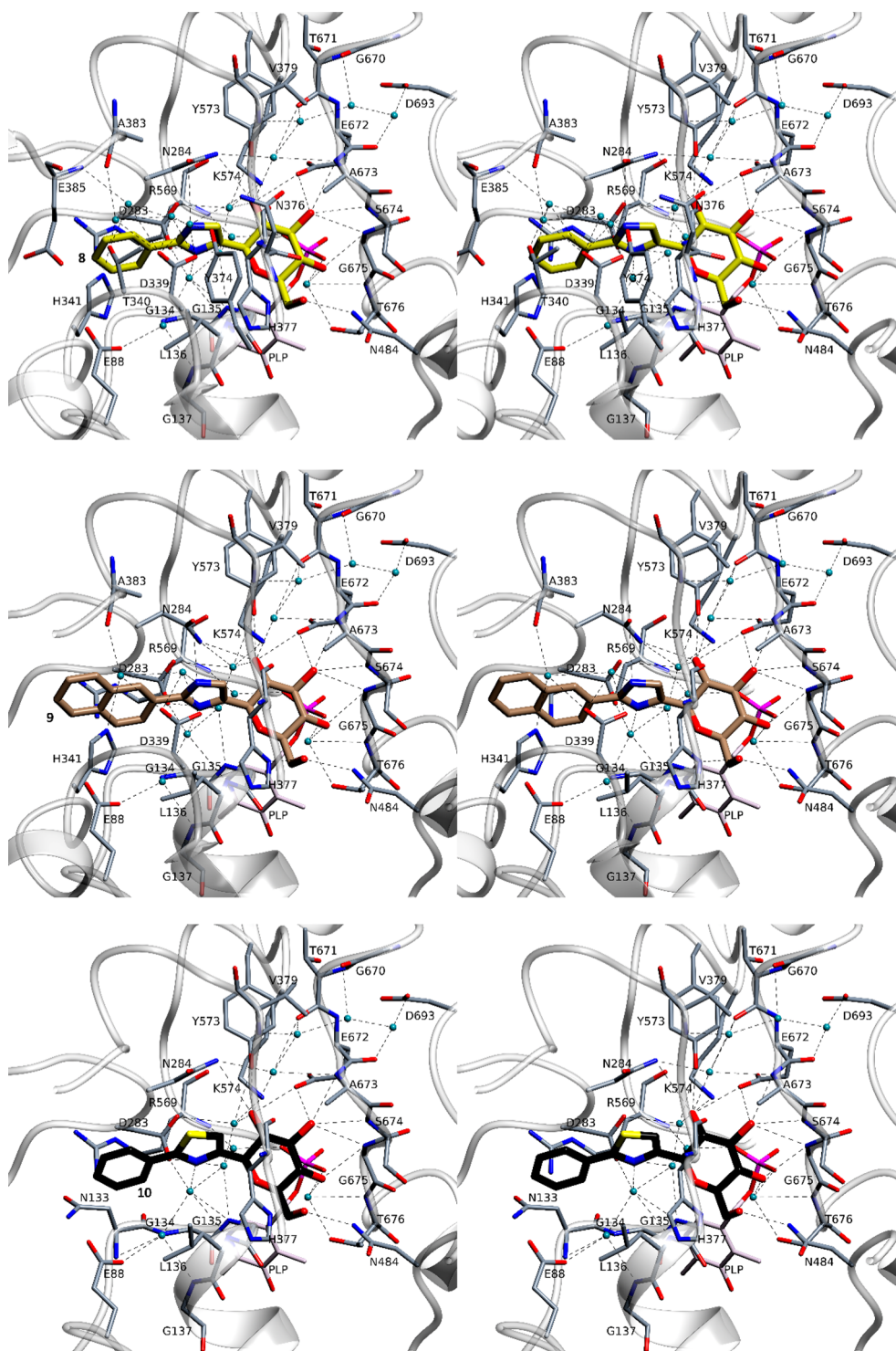


Fig. 4. A stereo diagram of the interactions of the ligands at the catalytic site (from top to down, 8, 9, 10, 11, 12, 13, and 14). The inhibitor molecules are shown as thick bonds, water molecules as cyan spheres and hydrogen bonds as dashed lines.

His341. These interactions seem to constitute the structural basis of the stronger inhibitory potency of **9** in comparison to **8**.

Structural comparison of the rmGPb **8** and **9** complexes, with the complexes of their isomers **1** and **2**²⁰ respectively, reveals that, although the isomers bind similarly (Fig. 6) and the water molecules mediating protein inhibitor interactions are conserved in all structures, the hydrogen bond of the linker nitrogen atom to His377 O in the **1** and **2** complexes has been replaced by a hydrogen bond to Asn284 OD1 in the **8** and **9** complexes (Table 3). Apart from the **1** and **2** complexes this

interaction to His377 O has been previously observed for the amide nitrogen of *N*-acetyl- β -D-glucopyranosylamine ($K_i = 32 \mu\text{M}$)^{11,55}, of glucopyranosylidene-spirohydantoin ($K_i = 3.1 \mu\text{M}$)^{56,57}, thiohydantoin ($K_i = 5.1 \mu\text{M}$)⁵⁸, β -D-glucopyranosyl formamide analogs ($K_i = 310\text{--}1800 \mu\text{M}$)⁵⁹, and *C*-(β -D-glucopyranosyl) benzimidazole ($K_i = 9 \mu\text{M}$)⁶⁰ and *C*-(β -D-glucopyranosyl) 1,2,4-triazoles ($K_i = 0.026\text{--}1.35 \mu\text{M}$)²², and the increased inhibitory potency of these compounds was attributed to this interaction. Loss of this interaction is significantly detrimental to the activity as shown for derivatives which

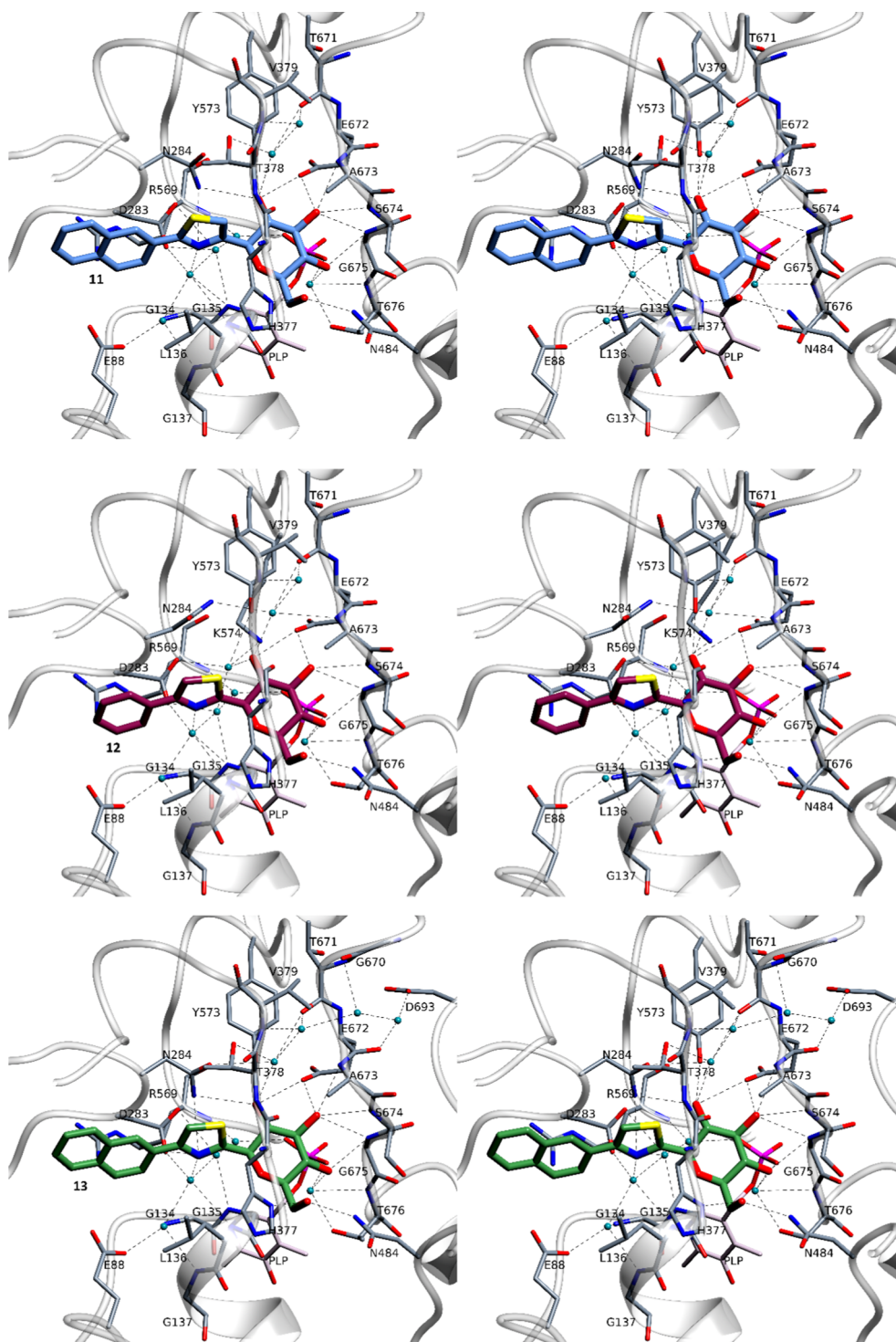


Fig. 4. (continued)

do not have a hydrogen donor at the 2 position (crystallographic numbering) of the heterocyclic linker²⁰. The distance of the hydrogen atom of N3 to Asn284 OD1 is 3.1 Å in **8** and **9** complexes. This distance is significantly longer than the distance of the hydrogen atom of N2 to His377 O (1.8 Å in **1** and **2** complexes²⁰). Furthermore, the N3-H-OD1 angle is $\sim 90^\circ$ in the **8** and **9** complexes while the N2-H-O angle is $\sim 170^\circ$ in the **1** and **2** complexes. The shorter distance and the almost linearity of the hydrogen bonds of **1** and **2** to His377 O in respect to those of **8** and **9** to Asn284 OD1 indicates that the hydrogen bonds of N2 to His377 O are stronger than those of N3 to Asn284 OD1^{61,62}. Furthermore, protein ligand hydrogen bond interactions are in general,

stronger when a protein main chain (like His377 O) rather than side chain (like Asn284 OD1) atom is involved⁶¹. This may offer a structural explanation for the increased inhibitory potency of **1** and **2** with respect to their isomers **8** and **9**, respectively. Accordingly, **14** displays significantly lower inhibitory potency ($K_i = 134.2 \mu\text{M}$) since neither of the nitrogen atoms of the tetrazole linker is capable to form a hydrogen bond to His377 O or Asn284 OD1.

Structural comparison of the rmGPb in complex with **7**²⁷ and **14** reveals that the two inhibitors bind quite differently in the active site (Fig. 7). In the rmGPb- **7** complex²⁷ a DMSO molecule (from the cryoprotectant solution) was found bound in the active site together

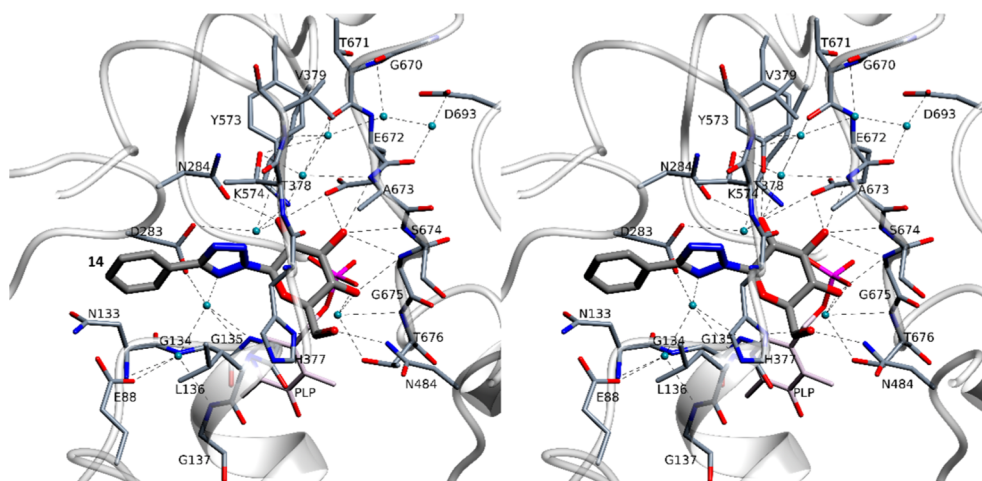


Fig. 4. (continued)

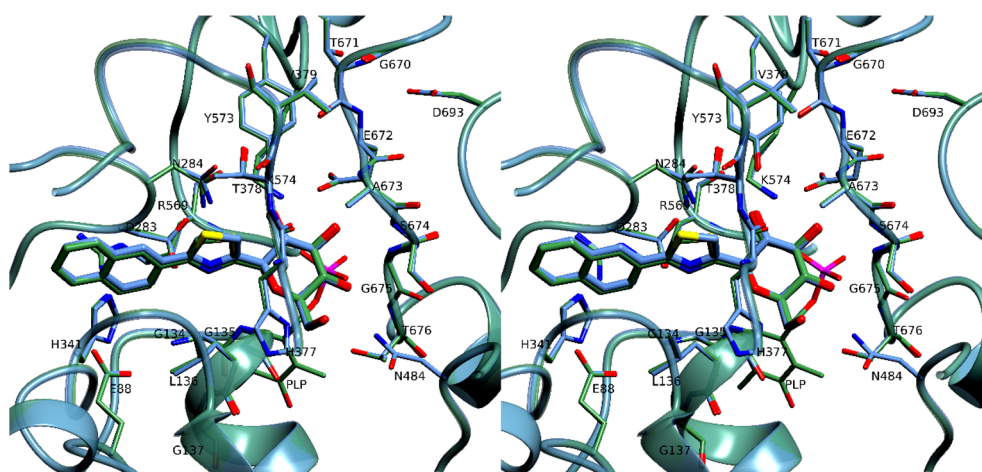


Fig. 5. Stereo diagrams of the superposition of the 13 and 11 complexes.

with the inhibitor. The binding of DMSO triggered a significant conformational change to the 280 s loop and seems that it also interferes with the binding of 7. Thus, the phenyl moiety attached to the heterocycle of 7 is rotated by $\sim 160^\circ$ with respect to its position in 14, and thus the corresponding atoms are 1–4 Å away. Inhibitors 7 and 14 are almost equipotent, comparing their K_i values, 162²⁸ or 151.3²⁷ and 162.3 μM for rmGPb, respectively (Table 2). Thus, it seems that the significant differences in the binding mode of 7 with respect to that of 14, may be an artefact of the rmGPb-7 complex data collection since these do not reflect in the potency of the two inhibitors.

4. Conclusions

C-Glucopyranosyl thiazoles, imidazoles and an *N*-glucopyranosyl tetrazole were studied and compared as to their inhibitory efficiency against isoforms of GP, *in vitro* and *ex vivo*. In contrast to 4(5)-glucopyranosyl-2-aryl-imidazoles which are potent inhibitors of rmGPb, rmGPa, and hGPa (the 2-naphthyl derivative is one of the most potent glucose analogue inhibitors), thiazoles are moderate inhibitors with K_i values in the range of 28–180 μM . The three most potent *in vitro* inhibitors, 8, 9 and 11 displayed also significant GP inhibitory potency at the cellular level. Structural studies of the rmGPb – inhibitor complexes by X-ray crystallography revealed the importance of the hydrogen bond interaction between the imidazole ring and the main chain carbonyl of His377. This hydrogen bond interaction when replaced by either a sulfur σ -hole bonding interaction or a hydrogen bond interaction to Asn284 OD1 leads to a decrease in the inhibitory activity due to

geometrical constraints. Finally, although the 2-glucosyl-tetrazole 14 seems to bind to rmGPb, differently from the 1,2,3-triazole 7, the two compounds are equipotent. Azoles and 1,2,3-triazoles containing compounds have a special importance in leads for drug design in various pathologies⁶³, and our study constitutes a significant contribution towards the design of novel antihyperglycaemic agents.

Declaration of Competing Interest

The authors declared that there is no conflict of interest.

Acknowledgments

We acknowledge support of this work by the project “The National Research Infrastructures on integrated biology, drug screening efforts and drug target functional characterization – INSPIRED-Thessaly” (MIS 5002550) which is implemented under the Action “Reinforcement of the Research and Innovation Infrastructure”, funded by the Operational Programme “Competitiveness, Entrepreneurship and Innovation” (NSRF 2014-2020) and co-financed by Greece and the European Union (European Regional Development Fund). E.K., O.P., and T.S. would like to acknowledge financial support from the Hellenic State Scholarships Foundation and the action “Support of human research resources through doctoral research” funded by the “Operational Programme Education and Lifelong Learning” co-funded by the European Social Fund (ESF) and National Resources. A.G.K. would like to acknowledge financial support from General Secretariat for Research and Technology

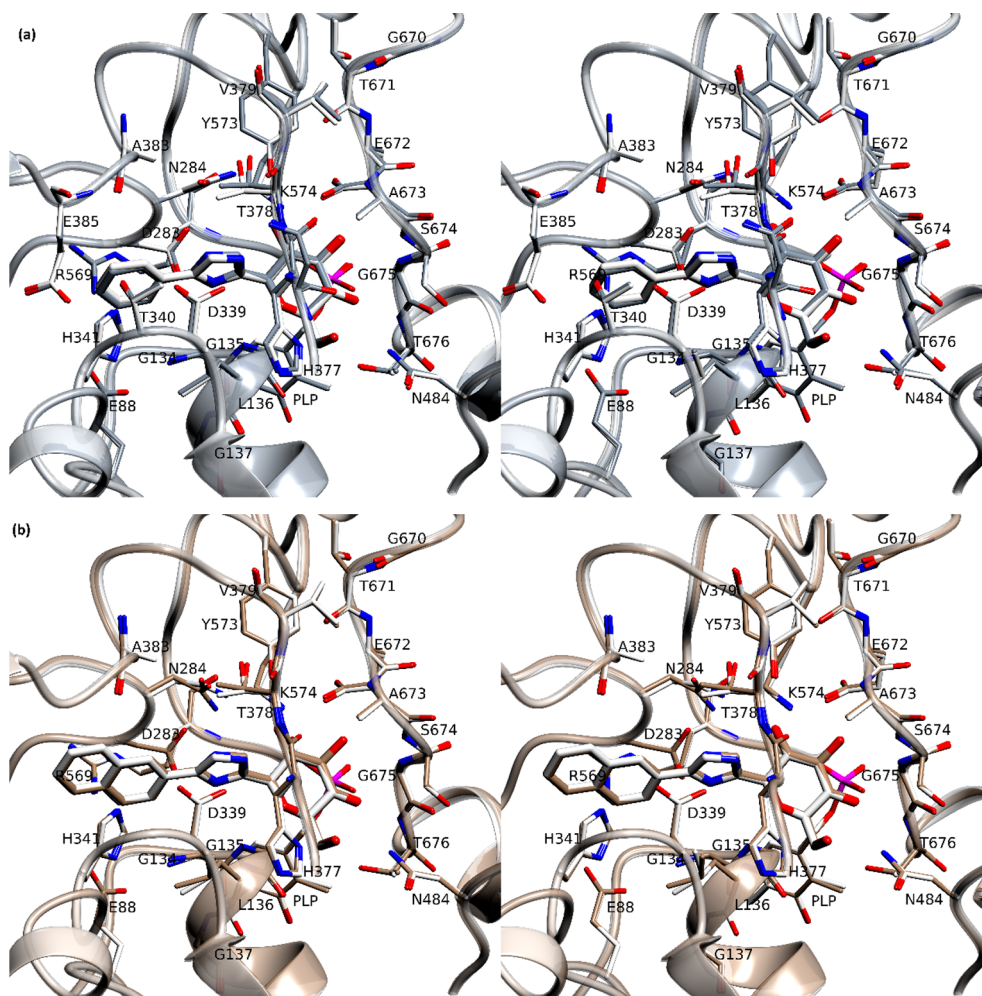


Fig. 6. Stereo diagrams of the superposition of the 1 and 8 (a) and 2 and 9 (b) complexes.

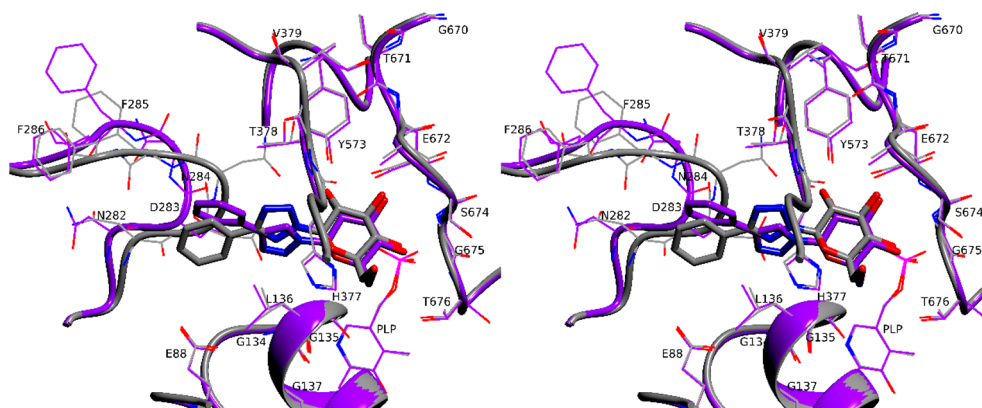


Fig. 7. Stereo diagrams of the superposition of 7 and 14 complexes.

(GSRT) and Hellenic Foundation for Research and Innovation (HFRI). The work was also supported by the National Research, Development and Innovation Office of Hungary (PD121406, FK125067) and by the EU co-financed by the European Regional Development Fund under the project GINOP-2.3.2-15-2016-00008.

References

- Oikonomakos NG. Glycogen phosphorylase as a molecular target for type 2 diabetes therapy. *Curr Protein Pept Sci.* 2002;3:561–586.
- Baker DJ, Timmons JA, Greenhaff PL. Glycogen phosphorylase inhibition in type 2 diabetes therapy – a systematic evaluation of metabolic and functional effects in rat skeletal muscle. *Diabetes.* 2005;54:2453–2459.
- Nagy L, Marton J, Vida A, et al. Glycogen phosphorylase inhibition improves beta cell function. *Br J Pharmacol.* 2018;175:301–319.
- Kerru N, Singh-Pillay A, Awolade P, Singh P. Current anti-diabetic agents and their molecular targets: a review. *Eur J Med Chem.* 2018;152:436–488.
- Somsak L. Glucose derived inhibitors of glycogen phosphorylase. *Compt Rend Chim.* 2011;14:211–223.
- Somsak L, Czifrak K, Toth M, et al. New inhibitors of glycogen phosphorylase as potential antidiabetic agents. *Curr Med Chem.* 2008;15:2933–2983.
- Hayes JM, Kantsadi AL, Leonidas DD. Natural products and their derivatives as inhibitors of glycogen phosphorylase: potential treatment for type 2 diabetes. *Phytochem Rev.* 2014;13:471–498.

8. Tsirkone VG, Tsoukala E, Lamprakis C, et al. 1-(3-Deoxy-3-fluoro-beta-D-glucopyranosyl) pyrimidine derivatives as inhibitors of glycogen phosphorylase b: Kinetic, crystallographic and modelling studies. *Bioorg Med Chem.* 2010;18:3413–3425.
9. Manta S, Xipnitou A, Kiritis C, et al. 3'-Axial CH₂OH Substitution on glucopyranose does not increase glycogen phosphorylase inhibitory potency. QM/MM-PBSA calculations suggest why. *Chem Biol Drug Des.* 2012;79:663–673.
10. Bokor E, Kyriakis E, Solovou TGA, et al. Nanomolar inhibitors of glycogen phosphorylase based on beta-D-glucosaminyl heterocycles: a combined synthetic, enzyme kinetic, and protein crystallography study. *J Med Chem.* 2017;60:9251–9262.
11. Watson KA, Mitchell EP, Johnson LN, et al. Glucose analogue inhibitors of glycogen phosphorylase: a study of alpha- and beta-C-glucosides and 1-thio-beta-D-glucose compounds. *Biochemistry.* 1994;33:5745–5758.
13. Barford D, Schwabe JW, Oikonomakos NG, et al. Channels at the catalytic site of glycogen phosphorylase b: binding and kinetic studies with the beta-glycosidase inhibitor D-gluconohydroxime-1,5-lactone N-phenylurethane. *Biochemistry.* 1988;27:6733–6741.
14. Barr D, Szennyes E, Bokor E, et al. Identification of C-beta-D-glucopyranosyl azole-type inhibitors of glycogen phosphorylase that reduce glycogenolysis in hepatocytes. In silico design, synthesis, in vitro kinetics, and ex vivo studies. *ACS Chem Biol.* 2019;14:1460–1470.
15. Docsa T, Czifrak K, Huse C, Somsak L, Gergely P. Effect of glucopyranosylidene-spirothiohydantoin on glycogen metabolism in liver tissues of streptozotocin-induced and obese diabetic rats. *Mol Med Report.* 2011;4:477–481.
16. Docsa T, Marics B, Nemeth J, et al. Insulin sensitivity is modified by a glycogen phosphorylase inhibitor: glucopyranosylidene-spiro-thiohydantoin in streptozotocin-induced diabetic rats. *Curr Top Med Chem.* 2015;15:2390–2394.
17. Goyard D, Konya B, Chajistamatiou AS, et al. Glucose-derived spiro-isoxazolines are anti-hyperglycemic agents against type 2 diabetes through glycogen phosphorylase inhibition. *Eur J Med Chem.* 2016;108:444–454.
18. Nagy L, Docsa T, Brunyánszki A, et al. Glycogen phosphorylase inhibitor N-(3,5-dimethyl-benzoyl)-N'-(beta-D-glucopyranosyl) urea improves glucose tolerance under normoglycemic and diabetic conditions through rearranging hepatic metabolism. *PLoS One.* 2013;8:e69420.
19. Bokor E, Kun S, Goyard D, et al. C-Glucopyranosyl arenes and heterarenes: synthetic methods and bioactivity focused on antidiabetic potential. *Chem Rev.* 2017;117:1687–1764.
20. Kantsadi AL, Bokor E, Kun S, et al. Synthetic, enzyme kinetic, and protein crystallographic studies of C-beta-D-glucopyranosyl pyrroles and imidazoles reveal and explain low nanomolar inhibition of human liver glycogen phosphorylase. *Eur J Med Chem.* 2016;123:737–745.
21. Kyriakis E, Solovou TGA, Kun S, et al. Probing the beta-pocket of the active site of human liver glycogen phosphorylase with 3-(C-beta-D-glucopyranosyl)-5-(4-substituted-phenyl)-1, 2, 4-triazole inhibitors. *Bioorg Chem.* 2018;77:485–493.
22. Kantsadi AL, Stravodimos GA, Kyriakis E, et al. van der Waals interactions govern C-beta-D-glucopyranosyl triazoles' nM inhibitory potency in human liver glycogen phosphorylase. *J Struct Biol.* 2017;199:57–67.
23. Kun S, Begum J, Kyriakis E, et al. A multidisciplinary study of 3-(beta-d-glucopyranosyl)-5-substituted-1,2,4-triazole derivatives as glycogen phosphorylase inhibitors: computation, synthesis, crystallography and kinetics reveal new potent inhibitors. *Eur J Med Chem.* 2018;147:266–278.
24. Bokor E, Kun S, Docsa T, Gergely P, Somsak L. 4(5)-Aryl-2-C-glucopyranosyl-imidazoles as New Nanomolar Glucose Analogue Inhibitors of Glycogen Phosphorylase. *ACS Med Chem Lett.* 2015;6:1215–1219.
25. Stravodimos GA, Chetter BA, Kyriakis E, et al. Phytogetic polyphenols as glycogen phosphorylase inhibitors: the potential of triterpenes and flavonoids for glycaemic control in type 2 diabetes. *Curr Med Chem.* 2017;24:384–403.
26. Kun S, Bokor E, Sipos Á, Docsa T, Somsak L. Synthesis of new C- and N-beta-D-glucopyranosyl derivatives of imidazole, 1,2,3-triazole and tetrazole, and their evaluation as inhibitors of glycogen phosphorylase. *Molecules.* 2018;23:666.
27. Chrysina ED, Bokor E, Alexacou KM, et al. Amide-1,2,3-triazole bioisosterism: the glycogen phosphorylase case. *Tetrahedron-Asymmetry.* 2009;20:733–740.
28. Bokor E, Docsa T, Gergely P, Somsak L. Synthesis of 1-(D-glucopyranosyl)-1,2,3-triazoles and their evaluation as glycogen phosphorylase inhibitors. *Bioorg Med Chem.* 2010;18:1171–1180.
29. Gimisis T. Synthesis of N-glucopyranosidic derivatives as potential inhibitors that bind at the catalytic site of glycogen phosphorylase. *Mini Rev Med Chem.* 2010;10:1127–1138.
30. Mirza A, Desai R, Reynisson J. Known drug space as a metric in exploring the boundaries of drug-like chemical space. *Eur J Med Chem.* 2009;44:5006–5011.
31. Fischer T, Koulas SM, Tsagkarakou AS, et al. High consistency of structure-based design and X-Ray crystallography: design, synthesis, kinetic evaluation and crystallographic binding mode determination of biphenyl-N-acyl-beta-D-glucopyranosylamines as glycogen phosphorylase inhibitors. *Molecules.* 2019;24:1322.
32. Leatherbarrow RJ. *GraFit version 4.06.* U.K.: Erithacus Software Ltd. Staines; 1998.
33. Kantsadi AL, Hayes JM, Manta S, et al. The sigma-hole phenomenon of halogen atoms forms the structural basis of the strong inhibitory potency of C5 halogen substituted glucopyranosyl nucleosides towards glycogen phosphorylase b. *ChemMedChem.* 2012;7:722–732.
34. Aiston S, Andersen B, Agius L. Glucose 6-phosphate regulates hepatic glycogenolysis through inactivation of phosphorylase. *Diabetes.* 2003;52:1333–1339.
35. Bradford MM. A rapid and sensitive method for the quantitation of microgram quantities of protein utilizing the principle of protein-dye binding. *Anal Biochem.* 1976;72:248–254.
36. Mosmann T. Rapid colorimetric assay for cellular growth and survival: application to proliferation and cytotoxicity assays. *J Immunol Methods.* 1983;65:55–63.
37. Agilent Technologies UK Ltd. *CrysAlisPro Software system*, Oxford, U.K.; 2011.
38. CCP4. The CCP4 suite : programs for protein crystallography. *Acta Crystallogr. D.* 1994;50:760–763.
39. Evans PR, Murshudov GN. How good are my data and what is the resolution? *Acta Crystallogr D Biol Crystallogr.* 2013;69:1204–1214.
40. Emsley P, Lohkamp B, Scott WG, Cowtan K. Features and development of Coot. *Acta Crystallogr D Biol Crystallogr.* 2010;66:486–501.
41. Schuttelkopf AW, van Aalten DMF. PRODRG: a tool for high-throughput crystallography of protein-ligand complexes. *Acta Crystallogr Section D-Biol Crystallogr.* 2004;60:1355–1363.
42. Joosten RP, Long F, Murshudov GN, Perrakis A. The PDB_REDO server for macromolecular structure model optimization. *Iucrj.* 2014;1:213–220.
43. Chen VB, Arendall 3rd WB, Headd JJ, et al. MolProbity: all-atom structure validation for macromolecular crystallography. *Acta Crystallogr D Biol Crystallogr.* 2010;66:12–21.
44. McNicholas S, Potterton E, Wilson KS, Noble ME. Presenting your structures: the CCP4mg molecular-graphics software. *Acta Crystallogr D Biol Crystallogr.* 2011;67:386–394.
45. Kun S, Bokor E, Varga G, et al. New synthesis of 3-(beta-D-glucopyranosyl)-5-substituted-1,2,4-triazoles, nanomolar inhibitors of glycogen phosphorylase. *Eur J Med Chem.* 2014;76:567–579.
46. Cer RZ, Mudunuri U, Stephens R, Lebeda FJ. IC50-to-Ki: a web-based tool for converting IC50 to Ki values for inhibitors of enzyme activity and ligand binding. *Nucleic Acids Res.* 2009;37:W441–W445.
47. Hudson JW, Golding GB, Crerar MM. Evolution of allosteric control in glycogen phosphorylase. *J Mol Biol.* 1993;234:700–721.
48. Rath VL, Ammirati M, LeMotte PK, et al. Activation of human liver glycogen phosphorylase by alteration of the secondary structure and packing of the catalytic core. *Mol Cell.* 2000;6:139–148.
49. Koebel MR, Cooper A, Schmadeke G, et al. S...O and S...N sulfur bonding interactions in protein-ligand complexes: empirical considerations and scoring function. *J Chem Inf Model.* 2016;56:2298–2309.
50. Barlow DJ, Thornton JM. Ion-pairs in proteins. *J Mol Biol.* 1983;168:867–885.
51. Leonidas DD, Chavali GB, Oikonomakos NG, et al. High-resolution crystal structures of ribonuclease A complexed with adenylic and uridylic nucleotide inhibitors. Implications for structure-based design of ribonucleolytic inhibitors. *Protein Sci.* 2003;12:2559–2574.
52. Fisher BM, Ha JH, Raines RT. Coulombic forces in protein-RNA interactions: Binding and cleavage by ribonuclease A and variants at Lys7, Arg10, and Lys66. *Biochemistry.* 1998;37:12121–12132.
53. Fisher BM, Schultz LW, Raines RT. Coulombic effects of remote subsites on the active site of ribonuclease A. *Biochemistry.* 1998;37:17386–17401.
54. Szabo KE, Kyriakis E, Psarra AG, Karra AG, Sipos A, Docsa T, Stravodimos GA, Katsidou E, Skamnaki VT, Liggri PGV, Zographos SE, Mandi A, Kiraly SB, Kurtan T, Leonidas DD, Somsak L. Glucopyranosylidene-spiro-imidazolinones, a New Ring System: Synthesis and Evaluation as Glycogen Phosphorylase Inhibitors by Enzyme Kinetics and X-ray Crystallography. *J Med Chem.* 2019;62:6116–6136.
55. Oikonomakos NG, Kontou M, Zographos SE, et al. N-acetyl-beta-D-glucopyranosylamine: a potent T-state inhibitor of glycogen phosphorylase. A comparison with alpha-D-glucose. *Protein Sci.* 1995;4:2469–2477.
56. Bichard CJF, Mitchell EP, Wormald MR, et al. Potent inhibition of glycogen phosphorylase by a spirohydantoin of glucopyranose - first pyranose analogs of hydantoin. *Tetrahedron Lett.* 1995;36:2145–2148.
57. Gregoriou M, Noble ME, Watson KA, et al. The structure of a glycogen phosphorylase glucopyranose spirohydantoin complex at 1.8 Å resolution and 100 K: the role of the water structure and its contribution to binding. *Protein Sci.* 1998;7:915–927.
58. Oikonomakos NG, Skamnaki VT, Osz E, et al. Kinetic and crystallographic studies of glucopyranosylidene spirothiohydantoin binding to glycogen phosphorylase b. *Bioorg Med Chem.* 2002;10:261–268.
59. Chrysina ED, Oikonomakos NG, Zographos SE, et al. Crystallographic studies on alpha- and beta-D-glucopyranosyl formamide analogues, inhibitors of glycogen phosphorylase. *Biocatal Biotransform.* 2003;21:233–242.
60. Chrysina ED, Kosmopoulou MN, Tiraidis C, et al. Kinetic and crystallographic studies on 2-(beta-D-glucopyranosyl)-5-methyl-1, 3, 4-oxadiazole, -benzothiazole, and -benzimidazole, inhibitors of muscle glycogen phosphorylase b. Evidence for a new binding site. *Protein Sci.* 2005;14:873–888.
61. Nittinger E, Inhester T, Bietz S, et al. Large-scale analysis of hydrogen bond interaction patterns in protein-ligand interfaces. *J Med Chem.* 2017;60:4245–4257.
62. Ferreira de Freitas R, Schapira M. A systematic analysis of atomic protein-ligand interactions in the PDB. *Medchemcomm.* 2017;8:1970–1981.
63. Bozorov K, Zhao J, Aisa HA. 1,2,3-Triazole-containing hybrids as leads in medicinal chemistry: A recent overview. *Bioorg Med Chem.* 2019;27:3511–3531.